J|A|C|S ARTICLES

Published on Web 06/03/2010

Evolution of Structure and Chemistry of Bimetallic Nanoparticle Catalysts under Reaction Conditions

Feng Tao,[†,‡,#] Michael E. Grass,[§] Yawen Zhang,[†,||] Derek R. Butcher,[†,‡] Funda Aksoy,[§,⊥] Shaul Aloni,[‡] Virginia Altoe,[‡] Selim Alayoglu,[†,‡] James R. Renzas,[†,‡] Chia-Kuang Tsung,[†] Zhongwei Zhu,[†,‡] Zhi Liu,[§] Miquel Salmeron,*[,‡] and Gabor A. Somorjai*[,†,‡]

Department of Chemistry, University of California, Berkeley, California 94720, Materials Science Division and Advanced Light Source, Lawrence Berkeley National Laboratory, Berkeley, California 94720, College of Chemistry and Molecular Engineering, Peking University, Beijing 100871, China, and Department of Physics, Çukurova University, 01330 Adana, Turkey

Received February 22, 2010; E-mail: MBSalmeron@lbl.gov; somorjai@berkeley.edu

Abstract: Three series of bimetallic nanoparticle catalysts (Rh_xPd_{1-x}, Rh_xPt_{1-x}, and Pd_xPt_{1-x}, $x = 0.2$, 0.5, 0.8) were synthesized using one-step colloidal chemistry. X-ray photoelectron spectroscopy (XPS) depth profiles using different X-ray energies and scanning transmission electron microscopy showed that the as-synthesized Rh_xPd_{1-x} and Pd_xPt_{1-x} nanoparticles have a core−shell structure whereas the Rh_xPt_{1-x} alloys are more homogeneous in structure. The evolution of their structures and chemistry under oxidizing and reducing conditions was studied with ambient-pressure XPS (AP-XPS) in the Torr pressure range. The Rh_xPd_{1-x} and Rh_xPt_{1-x} nanoparticles undergo reversible changes of surface composition and chemical state when the reactant gases change from oxidizing (NO or O_2 at 300 °C) to reducing (H_2 or CO at 300 °C) or catalytic (mixture of NO and CO at 300 °C). In contrast, no significant change in the distribution of the Pd and Pt atoms in the Pd_xPt_{1-x} nanoparticles was observed. The difference in restructuring behavior under these reaction conditions in the three series of bimetallic nanoparticle catalysts is correlated with the surface free energy of the metals and the heat of formation of the metallic oxides. The observation of structural evolution of bimetallic nanoparticles under different reaction conditions suggests the importance of in situ studies of surface structures of nanoparticle catalysts.

1. Introduction

Bimetallic catalysts are used in numerous reactions, including catalytic reforming,[1−4] pollution control,[1] and alcohol oxidation,[5] because of their superior catalytic activities and selectivities. The addition of a second metal is an important approach for tailoring the electronic and geometric structures to enhance the activity and selectivity.[5−9] Recent studies have demonstrated that the structure, composition, and oxidation state of the surface of bimetallic catalysts play a critical role in determining their catalytic properties. For example, bimetallic catalysts of Pt and 3d transition metals exhibit high activities and selectivities in several reactions relative to a pure Pt catalyst.[10−13] New bimetallic catalysts are being developed for applications such as fuel cells for efficient energy conversion from renewable resources, and this research is promising.[10−15]

Establishing the connection between the catalytic activity and selectivity of a catalyst and its physical and electronic structure under reaction conditions is crucial for the design of new catalysts.[16] In many cases, the structure and surface chemistry of the catalyst under reaction conditions are very different from those before and after a reaction, which are usually studied under high vacuum or at low temperature. To date, most structural and compositional studies of bimetallic catalysts have been performed ex situ. In most cases, the composition and chemical state of heterogeneous catalysts during reactions remain unknown.

One of the best techniques for determining surface composition and identifying chemical state is X-ray photoelectron spectroscopy (XPS). However, for a conventional XPS instrument, samples must be maintained in an environment with a

[†] University of California, Berkeley.
[‡] Materials Science Division, Lawrence Berkeley National Laboratory.
[§] Advanced Light Source, Lawrence Berkeley National Laboratory.
[||] Peking University.
[⊥] Çukurova University.
[#] Leaving for the University of Notre Dame.

(1) Somorjai, G. A. *Introduction to Surface Chemistry and Catalysis*; Wiley-VCH: New York, 1994.
(2) Burda, C.; Chen, X. B.; Narayanan, R.; El-Sayed, M. A. *Chem. Rev.* **2005**, *105*, 1025.
(3) Campbell, C. T. *Annu. Rev. Phys. Chem.* **1990**, *41*, 775.
(4) Rodriguez, J. A.; Goodman, D. W. *Science* **1992**, *257*, 897.
(5) Enache, D. I.; Edwards, J. K.; Landon, P.; Solsona-Espriu, B.; Carley, A. F.; Herzing, A. A.; Watanabe, M.; Kiely, C. J.; Knight, D. W.; Hutchings, G. J. *Science* **2006**, *311*, 362.
(6) Bligaard, T.; Nørskov, J. K.; Rossmeisl, J.; Christensen, C. H. *Nat. Chem.* **2009**, *1*, 37.
(7) Nørskov, J. K.; Christensen, C. H. *Science* **2006**, *312*, 1322.
(8) Nørskov, J. K. *Nature* **2001**, *414*, 405.
(9) Besenbacher, F.; Chorkendorff, I.; Clausen, B. S.; Hammer, B.; Molenbroek, A. M.; Nørskov, J. K.; Stensgaard, I. *Science* **1998**, *279*, 1913.

 © 2010 American Chemical Society

pressure lower than 10^{-7} Torr (high vacuum) because of the limited elastic mean free path of photoelectrons in gaseous environments with relatively higher pressures.[17] We used ambient-pressure XPS (AP-XPS), which allows for studies of catalysts in environments having reactants in the Torr pressure range and temperatures of up to several hundred degrees Celsius.[16−18] In addition, the tunable X-ray energy provided by synchrotron sources makes it possible to obtain a depth profile of atomic composition near the surface under reaction conditions.

In this paper, we present the results of our studies of the synthesis of Rh_xPd_{1-x}, Rh_xPt_{1-x}, and Pd_xPt_{1-x} bimetallic nanoparticles and the distribution of the constituent elements of the as-synthesized nanoparticle catalysts. In addition to XPS, we also used energy-dispersive X-ray (EDX) analyses in a transmission electron microscope in scanning mode to independently identify the spatial distribution of the constituent elements. We studied the evolution of composition and chemical state in the surface region of these bimetallic nanoparticle catalysts under oxidizing (NO or O_2) and reducing (CO or H_2) conditions and in catalytic reactions ($CO + NO \rightarrow N_2/N_2O + CO_2$) at a pressure of 100 mTorr of each gas at 300 °C. These reactant gases were selected because they participate in numerous reactions in energy conversion and pollution control.[1,16]

2. Experimental Section

The Rh_xPd_{1-x}, Rh_xPt_{1-x}, and Pd_xPt_{1-x} nanoparticles ($x = 0.2$, 0.5, 0.8) were synthesized in a one-step process involving the reduction of two precursors under Ar gas using poly(vinylpyrrolidone) (PVP) as a surfactant. To synthesize Rh_xPd_{1-x} nanoparticles, $Rh(acac)_3$ and $Pd(acac)_2$ (acac = acetylacetonate) with specific atomic ratios and PVP were added to 1,4-butanediol in a 50 mL three-neck flask at room temperature. The stock solution was heated to 50 °C and evacuated for 20 min under magnetic stirring to remove water and oxygen; this formed an optically transparent orange-yellow solution. The flask was then heated to 220 °C at a rate of 10 °C/min and maintained at this temperature (±2 °C) for 1.5 h under Ar gas. When the reaction was complete, the solution was cooled to room temperature. Next, excess acetone was added to the solution, producing a cloudy black suspension. The suspension was separated, and the black product was collected by discarding the colorless supernatant. The precipitated Rh_xPd_{1-x} nanoparticles were washed with acetone and then redispersed in ethanol. Similar synthetic procedures were used for Rh_xPt_{1-x} and Pd_xPt_{1-x} nanoparticles. The shape, size, and crystallinity of the nanoparticles were examined by high-resolution transmission electron microscopy (HRTEM; Jeol 2100F, 200 kV) and X-ray diffraction (XRD; Bruker D8 GADDS).

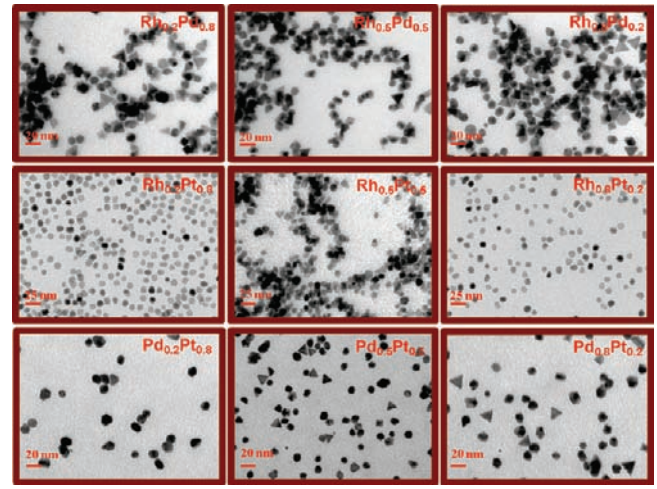

Figure 1. Representative TEM images of Rh_xPd_{1-x}, Rh_xPt_{1-x}, and Pd_xPt_{1-x} bimetallic nanoparticles before any reactions. Nanoparticle sizes: Rh_xPd_{1-x}, ~15 nm; Rh_xPt_{1-x}, 8−11 nm; Pd_xPt_{1-x}, ~16 nm.

Monolayers of bimetallic nanoparticles on silicon wafers were prepared by placing a certain amount of a chloroform solution of nanoparticles onto the water subphase of a Langmuir−Blodgett (LB) trough (Nima Technology, M611) at room temperature.[19] The resulting layer was compressed at a rate of 15 cm^2/min and transferred onto a silicon wafer using the Langmuir−Schäffer horizontal lift-off method. The nanoparticle films on the silicon wafers were examined with scanning electron microscopy (SEM). XPS spectra from the Rh 3d, Pd 3d, and Pt 4f core levels were obtained by AP-XPS at the Advanced Light Source at Berkeley.[18] The peak intensities of these photoemission features were used to determine the atomic fractions of the two elements after calibration using the photoionization cross sections corresponding to the X-ray energies used.[20]

3. Results

3.1. Structure and Chemistry of Nanoparticles before Reaction. The sizes of the as-synthesized Rh_xPd_{1-x}, Rh_xPt_{1-x}, and Pd_xPt_{1-x} nanoparticles were ~15, 8−11, and ~16.0 nm, respectively. Figure 1 shows TEM images of Rh_xPd_{1-x}, Rh_xPt_{1-x}, and Pd_xPt_{1-x} ($x = 0.2$, 0.5, 0.8) nanoparticles. The EDX spectra of single nanoparticles reveal the presence of the two component elements, and the spatial mapping images of the Rh Kα and Pd Kα emissions (Figure 2) clearly show the core−shell structure of the Rh_xPd_{1-x} nanoparticles. Here, the core−shell structure involves a Rh-rich shell and a Pd-rich core. Notably, panels (b3) and (b4) of Figure 2 reveal the core−shell structure of the $Rh_{0.5}Pd_{0.5}$ nanoparticles even when their shapes are different. Similar images for $Rh_{0.8}Pd_{0.2}$ (Figure 2a3,a4) and $Rh_{0.2}Pd_{0.8}$

(10) Stamenkovic, V. R.; Fowler, B.; Mun, B. S.; Wang, G.; Ross, P. N.; Lucas, C. A.; Markovic, N. M. *Science* **2007**, *315*, 493.
(11) (a) Alayoglu, S.; Nilekar, A. U.; Mavrikakis, M.; Eichhorn, B. *Nat. Mater.* **2008**, *7*, 333. (b) Zhou, S.; Varughese, B.; Eichhorn, B.; Jackson, G.; McIlwrath, K. *Angew. Chem., Int. Ed.* **2005**, *44*, 45539.
(12) Knudsen, J.; Nilekar, A. U.; Vang, R. T.; Schnadt, J.; Kunkes, E. L.; Dumesic, J. A.; Mavrikakis, M.; Besenbacher, F. *J. Am. Chem. Soc.* **2007**, *129*, 6485.
(13) Murillo, L. E.; Goda, A. M.; Chen, J. G. *J. Am. Chem. Soc.* **2007**, *129*, 7101.
(14) (a) Zhou, W. P.; Yang, X. F.; Vukmirovic, M. B.; Koel, B. E.; Jiao, J.; Peng, G. W.; Mavrikakis, M.; Adzic, R. R. *J. Am. Chem. Soc.* **2009**, *131*, 12755. (b) Stolbov, S.; Ortigoza, M. A.; Adzic, R.; Rahman, T. S. *J. Chem. Phys.* **2009**, *130*, 124714. (c) Kowal, A.; Li, M.; Shao, M.; Sasaki, K.; Vukmirovic, M. B.; Zhang, J.; Marinkovic, N. S.; Liu, P.; Frenkel, A. I.; Adzic, R. R. *Nat. Mater.* **2009**, *8*, 325. (d) Huber, G. W.; Shabaker, J. W.; Dumesic, J. A. *Science* **2003**, *300*, 2075. (e) Chen, P.; Xu, W. L.; Zhou, X. C.; Panda, D.; Kalininskiy, A. *Chem. Phys. Lett.* **2009**, *470*, 151.
(15) Kolb, G. *Fuel Processing: for Fuel Cells*; Wiley-VCH: Weinheim, Germany, 2008.
(16) (a) Tao, F.; Dag, S.; Wang, L. W.; Liu, Z.; Butcher, D. R.; Bluhm, H.; Salmeron, M.; Somorjai, G. A. *Science* **2010**, *327*, 850. (b) Altman, M. S. *Science* **2010**, *327*, 789. (c) Somorjai, G. A.; Tao, F.; Park, J. *Top. Catal.* **2008**, *47*, 1.
(17) (a) Hufner, S. *Photoelectron Spectroscopy*, 3rd ed.; Springer, Berlin, 2005. (b) Ambient pressure XPS using household X-ray sources is available from a couple of manufacturers of analytical instruments.
(18) (a) Salmeron, M.; Schlögl, R. *Surf. Sci. Rep.* **2008**, *63*, 169. (b) Ogletree, D. F.; Bluhm, H.; Lebedev, G.; Fadley, C. S.; Hussain, Z.; Salmeron, M. *Rev. Sci. Instrum.* **2002**, *73*, 3872.
(19) (a) Zhang, Y. W.; Grass, M. E.; Kuhn, J. N.; Tao, F.; Habas, S. E.; Huang, W. Y.; Yang, P. D.; Somorjai, G. A. *J. Am. Chem. Soc.* **2008**, *130*, 5868. (b) Zhang, Y. W.; Grass, M. E.; Habas, S. E.; Tao, F.; Zhang, T. F.; Yang, P. D.; Somorjai, G. A. *J. Phys. Chem. C* **2007**, *111*, 12243. (c) Tao, F.; Dag, S.; Wang, L. W.; Liu, Z.; Salmeron, M.; Somorjai, G. A. *Nano Lett.* **2009**, *9*, 2167.
(20) Yeh, J. J.; Lindau, I. L. *At. Data Nucl. Data Tables* **1985**, *32*, 1.

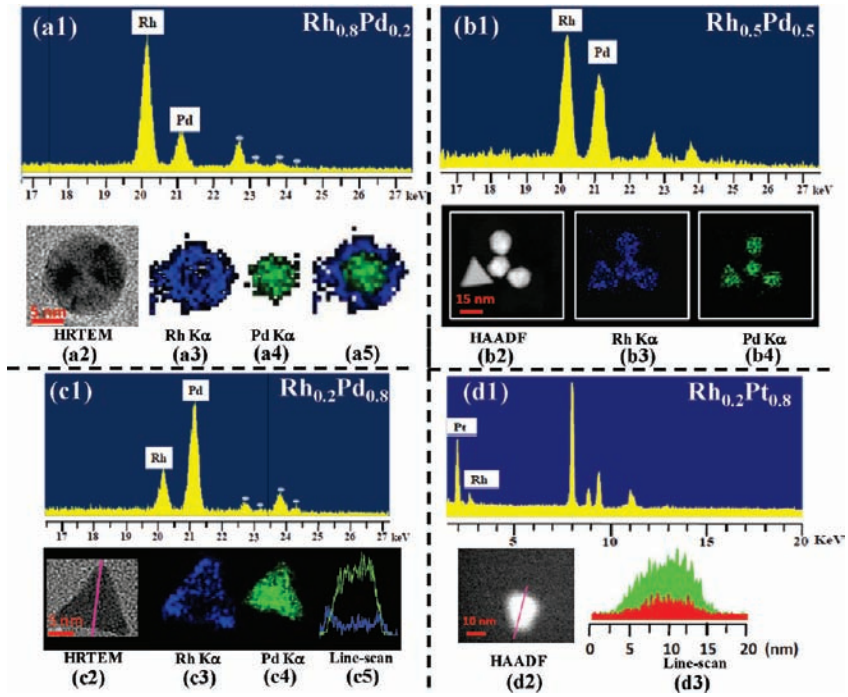

Figure 2. (a1) EDX spectrum of a single $Rh_{0.8}Pd_{0.2}$ nanoparticle; (a2−a4) HRTEM image of a $Rh_{0.8}Pd_{0.2}$ nanoparticle (a2) and corresponding elemental mapping images obtained from (a3) Rh Kα and (a4) Pd Kα emissions; (a5) superposition of (blue) Rh and (green) Pd distributions for a single $Rh_{0.8}Pd_{0.2}$ nanoparticle, illustrating the core−shell structure. (b1) EDX spectrum of a single $Rh_{0.5}Pd_{0.5}$ nanoparticle; (b2−b4) high-angle annual dark-field (HAADF) image of four adjacent $Rh_{0.5}Pd_{0.5}$ nanoparticles (b2) and corresponding elemental mapping images from (b3) Rh Kα and (b4) Pd Kα emissions from the four nanoparticles. (c1) EDX spectrum of single $Rh_{0.2}Pd_{0.8}$ nanoparticle; (c2−c4) HRTEM image of a representative $Rh_{0.2}Pd_{0.8}$ nanoparticle (c2) and its elemental mapping images from (c3) Rh Kα and (c4) Pd Kα emissions; (c5) line-scan profiles (green line for Pd and blue line for Rh) of the elemental distribution along the pink line shown in (c2). (d1) EDX spectrum of a $Rh_{0.2}Pt_{0.8}$ nanoparticle; (d2) HAADF image of a $Rh_{0.2}Pt_{0.8}$ nanoparticle; (d3) line-scan profile (green for Pt and red for Rh) along the pink line shown in (d2).

(Figure 2c3,c4) show that the atomic fraction of Rh is relatively high in the surface region and low in deeper layers. Thus, the Rh_xPd_{1-x} ($x = 0.2, 0.5, 0.8$) nanoparticles have Rh-rich shells and Pd-rich cores. However, the Rh Kα and Pt Kα line profiles for a single Rh_xPt_{1-x} nanoparticle, such as $Rh_{0.2}Pt_{0.8}$ (Figure 2d2,d3) do not suggest a distinct core−shell structure.

The distributions of the constituent elements in the nanoparticle catalysts in the LB films on silicon substrates before reactions were studied by XPS, using X-ray energies of 645, 850, and 1486.6 eV to generate photoelectrons from the Rh 3d and Pd 3d core levels with kinetic energies of ∼310, ∼510, and ∼1150 eV, respectively. The mean free paths (IMFPs) of these photoelectrons were ∼0.7, ∼1.0, and ∼1.6 nm, respectively.[21] For Rh_xPt_{1-x} and Pd_xPt_{1-x} nanoparticles, the X-ray energies were chosen to be 645 and 850 eV to excite the Rh 3d and Pd 3d core-level electrons, respectively, and 350 and 600 eV, respectively, to excite the Pt 4f core-level electrons; this ensured that the kinetic energies (or IMFPs) of photoelectrons emitted from core levels of the two constituent elements in the same nanoparticle catalyst were similar. After correction for the incident flux and photoionization cross section, the measured intensities provided depth-weighted average compositions of the nanoparticles.

As shown in Figure 3, the measured atomic fractions of Rh and Pd in the as-synthesized Rh_xPd_{1-x} nanoparticles varied as a function of depth. For example, the Rh atomic fractions in the $Rh_{0.2}Pd_{0.8}$ nanoparticles were ∼56, ∼42, and ∼18% at excitation energies corresponding to IMFPs of ∼0.7, ∼1.0, and ∼1.6 nm, respectively. The fractions were ∼92, ∼84, and ∼56% for $Rh_{0.5}Pd_{0.5}$ nanoparticles and ∼95, ∼91, and ∼81% for $Rh_{0.8}Pd_{0.2}$ nanoparticles. Similar to the case of Rh_xPd_{1-x}, the atomic fractions of Pd and Pt in the $Pd_{0.5}Pt_{0.5}$ nanoparticles (Figure 4b) exhibited a significant dependence on depth, with the shell region enriched in Pd. Figure 5 shows the measured atomic fractions of Rh and Pt at different incident photon energies for as-synthesized Rh_xPt_{1-x} nanoparticles. The depth dependence of the atomic fractions of Rh and Pt in the Rh_xPt_{1-x} nanoparticles is much weaker than in the Rh_xPd_{1-x} and Pd_xPt_{1-x} cases, suggesting that the Rh_xPt_{1-x} nanoparticles were predominately a homogeneous solid solution of Rh and Pt.

3.2. Structure and Surface Chemistry of Nanoparticle Catalysts under Reaction Conditions. Before the reactions were performed, the PVP surfactant was removed by outgassing the samples at 150 °C under high vacuum and subsequent annealing to 150−200 °C under a low pressure of oxygen or nitric oxide (1×10^{-5} Torr). This pretreatment removed the majority of PVP, as confirmed by the change in the relative intensity of the C 1s and substrate Si 2p peaks. Upon this pretreatment, there was no obvious change in the atomic fractions of the two constituent elements of the nanoparticles. The atomic fractions and oxidation states of Rh_xPd_{1-x}, Rh_xPt_{1-x}, and Pd_xPt_{1-x} nanoparticle catalysts were determined in situ using AP-XPS at 300 °C under 100 mTorr H_2, CO, NO, or O_2 or a mixture of 100 mTorr CO and 100 mTorr NO.

Figure 6 shows the atomic fractions of Rh and Pd in the surface regions (approximately from the surface to the third or fourth layer) of $Rh_{0.2}Pd_{0.8}$, $Rh_{0.5}Pd_{0.5}$, and $Rh_{0.8}Pd_{0.2}$ catalysts

(21) Powell, C. J.; Jablonski, A. *NIST Electron Inelastic Mean Free Path Database*, version 1.1; National Institute of Standards and Technology: Gaithersburg, MD, 2002. (a) Shirinyan, A. S.; Gusak, A. M.; Wautelet, M. *Acta Mater.* **2005**, *53*, 5025. (b) Shirinyan, A. S.; Gusak, A. M. *Philos. Mag.* **2004**, *84*, 579.

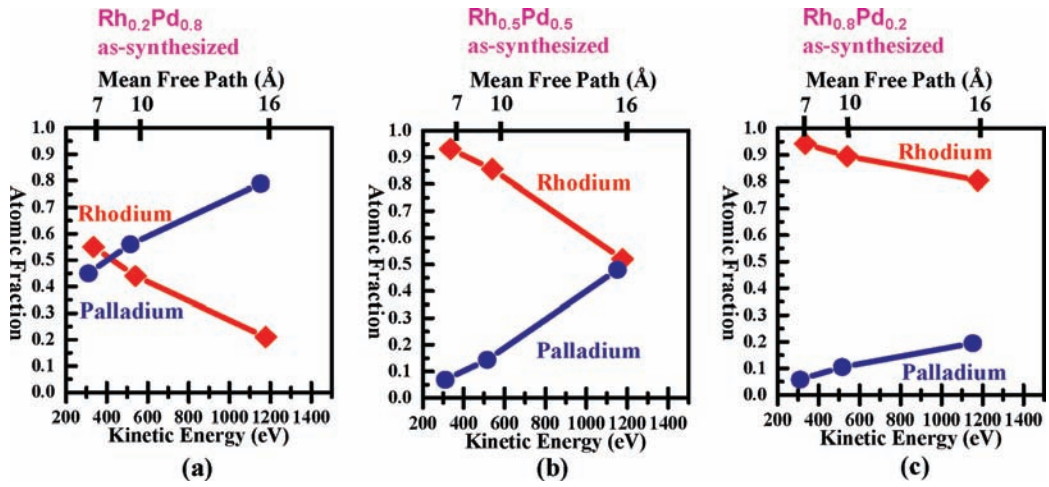

Figure 3. Dependence of rhodium and palladium atomic fractions of as-synthesized Rh_xPd_{1-x} nanoparticles (~15 nm) measured at 25 °C in vacuum (<1 × 10^{-8} Torr) as a function of photoelectron kinetic energy and mean free path: (a) $Rh_{0.2}Pd_{0.8}$; (b) $Rh_{0.5}Pd_{0.5}$; (c) $Rh_{0.8}Pd_{0.2}$.

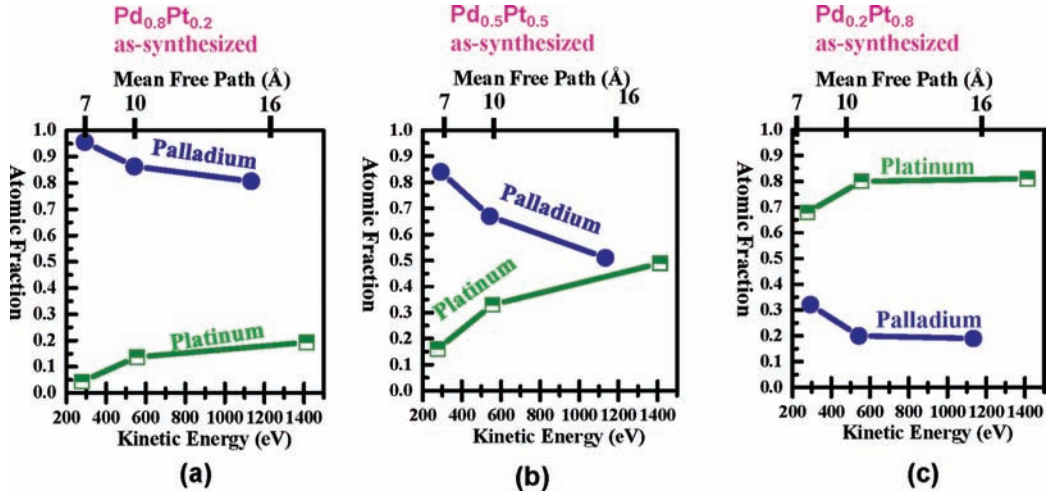

Figure 4. Dependence of palladium and platinum atomic fractions on the analysis depth in as-synthesized Pd_xPt_{1-x} nanoparticles (~16 nm), as measured using XPS at 25 °C in vacuum (<1 × 10^{-8} Torr) as a function of photoelectron kinetic energy and mean free path: (a) $Pd_{0.8}Pt_{0.2}$; (b) $Pd_{0.5}Pt_{0.5}$; (c) $Pd_{0.2}Pt_{0.8}$.

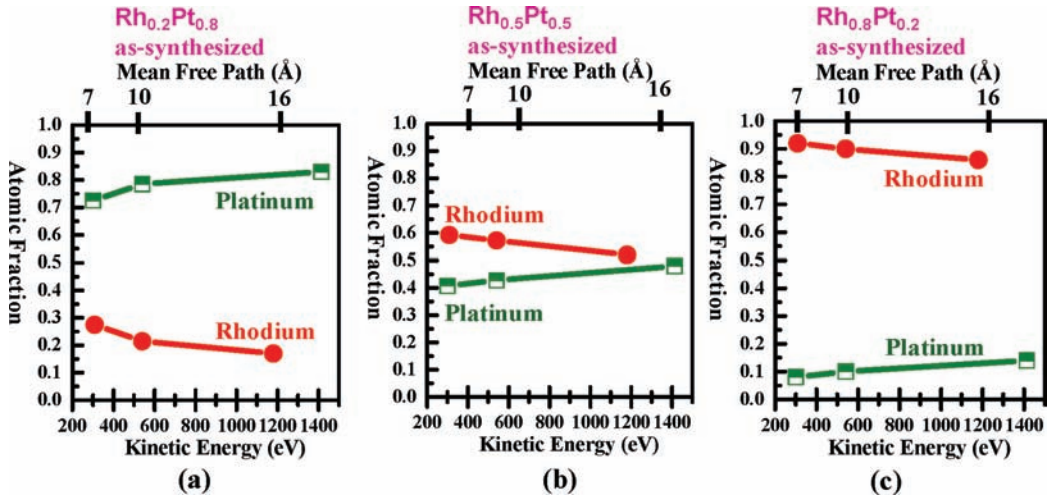

Figure 5. Dependence of rhodium and platinum atomic fractions of as-synthesized Rh_xPt_{1-x} nanoparticles (8−11 nm) measured using XPS at 25 °C in vacuum (<1 × 10^{-8} Torr) as a function of photoelectron kinetic energy and mean free path: (a) $Rh_{0.2}Pt_{0.8}$; (b) $Rh_{0.5}Pt_{0.5}$; (c) $Rh_{0.8}Pt_{0.2}$.

in a sequence of reaction conditions varying from oxidizing (NO) to reducing (CO) or catalytic (NO + CO). These changes were reversible when the environment was switched from oxidizing back to reducing or catalytic conditions and could be repeated over several cycles. The atomic fraction of Rh increased when the reducing environment was changed to an oxidizing

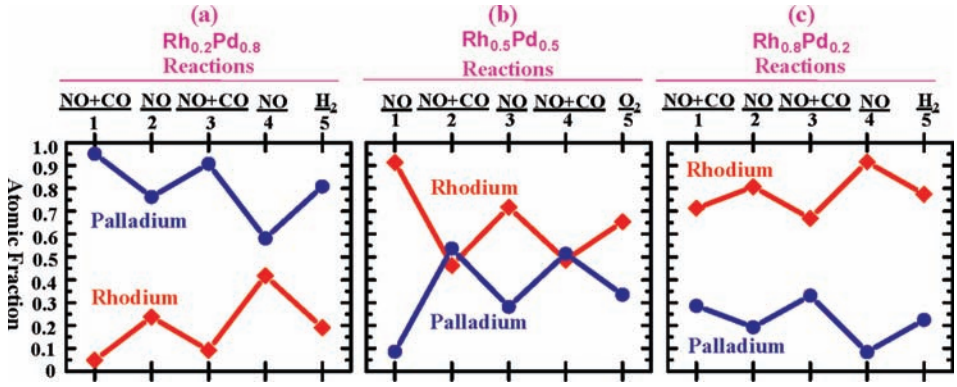

Figure 6. Evolution of rhodium and palladium atomic fractions in Rh_xPd_{1-x} nanoparticles (~15 nm) at 300 °C under oxidizing conditions (100 mTorr NO or O_2), reducing conditions (100 mTorr H_2), and catalytic conditions (100 mTorr NO and 100 mTorr CO), as denoted on the horizontal axis. All of the atomic fractions were obtained using an X-ray energy of 645 eV for Rh 3d and Pd 3d, which generated photoelectrons with a mean free path of ~0.7 nm.

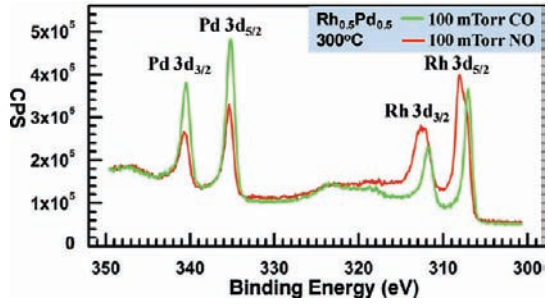

Figure 7. Rh 3d and Pd 3d XPS spectra of $Rh_{0.5}Pd_{0.5}$ nanoparticles (~15 nm) collected in 100 mTorr NO (red spectrum) and 100 mTorr CO (green spectrum) reaction environments at 300 °C. The X-ray energy used for Rh 3d, Pd 3d, Si 2p, and the Fermi level was 645 eV. The binding energies were calibrated with the Si 2p core level of metallic silicon and the Fermi levels at the same X-ray energies under the same reaction conditions.

one. It decreased again when the reaction conditions were changed to reducing (CO, H_2, or CO + NO). The oscillations of the surface compositions decayed slightly after a few cycles. This could result from thermal diffusion of carbon atoms or carbon-containing species left by PVP, as the PVP surfactant was not completely removed under the current pretreatment. The carbon species in the surface region could change chemical composition and chemical states to some extent after a few cycles of restructuring, weakening the segregation behavior.

Figure 7 presents the Rh 3d and Pd 3d XPS spectra for $Rh_{0.5}Pd_{0.5}$ bimetallic nanoparticles collected in reaction environments of 100 mTorr NO (red line) and 100 mTorr CO (green line) at 300 °C. The Rh 3d photoemission features indicate that rhodium oxide was formed in the presence of NO and was reduced back to metallic Rh in the presence of CO. The different relative Rh photoemission intensities under different conditions show the restructuring in the shell subphase.

The structural evolution in the surface region of Rh_xPt_{1-x} nanoparticles under reaction conditions was studied at 300 °C in environments with various reactants as well. Although the structure of the synthesized nanoparticles before reactions was not core−shell (Figures 2d and 5), they were still restructured when the gas conditions were switched between reducing and oxidizing (Figure 8). Similar to the Rh_xPd_{1-x} case, Rh was segregated to the surface of the Rh_xPt_{1-x} nanoparticles in oxidizing environments. The segregation of Rh under oxidizing conditions can be explained by the formation of rhodium oxide, which is energetically more stable than the oxides of Pd and

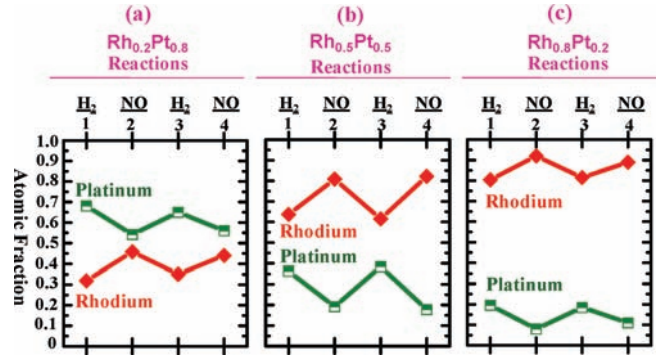

Figure 8. Evolution of rhodium and platinum atomic fractions of Rh_xPt_{1-x} nanoparticles (8−11 nm) at 300 °C under reducing conditions (100 mTorr H_2) and oxidizing conditions (100 mTorr NO), as denoted on the horizontal axis. All of the atomic fractions in this figure were obtained using X-ray energies of 645 eV for Rh 3d and 380 eV for Pt 4f, which generated photoelectrons with a mean free path of ~0.7 nm.

Pt,[22−25] on the basis of analyses of the Rh 3d, Pd 3d, and Pt 4f photoemission features of these nanoparticle catalysts collected under reaction conditions. The molar free energy of formation of $RhO_{3/2}$ is −39 kcal mol^{-1} and that of PdO is −21.4 kcal mol^{-1}.[22,23] In addition, for Rh−Pd bimetallic nanoparticles, the formation of rhodium oxide on the surface prevents Pd in deep layers from segregating to the surface. The low dissociation temperature of NO on Rh relative to Pd could be another driving force for the preferential oxidation of Rh.

Under reducing conditions, RhO_x is reduced to the metallic state; Pd in Rh_xPd_{1-x} and Pt in Rh_xPt_{1-x} segregate to the surface under these conditions because both metals have a lower surface free energy than Rh [Rh(100), 2.9 J m^{-2}; Pt(100), 2.48 J m^{-2}; Pd(100), 1.90 J m^{-2}].[24] Thus, the surface free energy of the metal determines the atomic segregation under reducing conditions, while the formation energy of metallic oxides dominates the restructuring under oxidizing conditions at 300 °C. The variation of atomic fractions in the surface region of the Rh_xPt_{1-x} nanoparticles between reducing and oxidizing conditions is

(22) (a) Bichowsky, F. R.; Rossini, F. D. *The Thermochemistry of the Chemical Substances*; Reinhold Publishing: New York, 1936. (b) Salmeron, M.; Brewer, L.; Somorjai, G. A. *Surf. Sci.* **1981**, *112*, 207.
(23) Samsonov, G. V. *The Oxide Handbook*, 2nd ed.; IVI/Plenum: New York, 1982.
(24) Skriver, H. L.; Rosengaard, N. M. *Phys. Rev. B* **1992**, *46*, 7157.
(25) Edwards, J. K.; Solsona, B.; Ntainjua, E.; Carley, A. F.; Herzing, A. A.; Kiely, C. J.; Hutchings, G. J. *Science* **2009**, *323*, 1037.

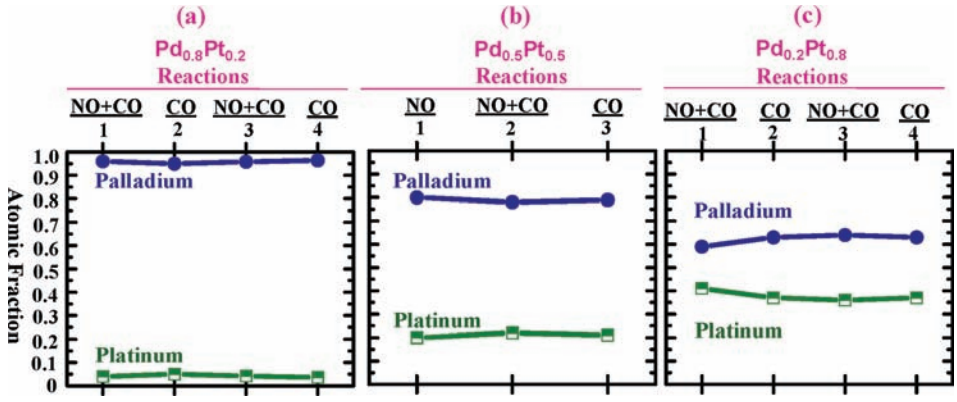

Figure 9. Evolution of palladium and platinum atomic fractions for Pd_xPt_{1-x} nanoparticles (~16 nm) at 300 °C under oxidizing (100 mTorr NO), reducing (100 mTorr CO), and catalytic (100 mTorr NO and 100 mTorr CO) conditions. The horizontal axis represents different reaction conditions. All of the atomic fractions were obtained using X-ray energies of 645 eV for Pd 3d and 380 eV for Pt 4f, which generated photoelectrons with a mean free path of ~0.7 nm.

smaller than that of the Rh_xPd_{1-x} nanoparticles between the two conditions (Figures 6 and 8).

Similar studies show that the changes in the compositions of Pt and Pd in the surface region of the Pd_xPt_{1-x} nanoparticles are much weaker than those in Rh_xPd_{1-x} and Rh_xPt_{1-x} nanoparticles. As shown in Figure 9, the atomic fractions of Pd and Pt did not show a significant change when the environment was switched between oxidizing and reducing (or catalytic) conditions. Under reducing conditions, Pd has a lower surface free energy than Pt;[22−25] thus, Pd segregates to the surface, and the surface region becomes Pd-rich. Since the oxidization of Pd is more favorable than that of Pt, Pt does not segregate to the surface under oxidizing conditions. Therefore, the atomic fractions of Pd and Pt in Pd_xPt_{1-x} remain nearly constant under both oxidizing and reducing conditions at 300 °C, though palladium oxide is formed and reduced under oxidizing and reducing conditions, respectively.

The restructuring of bimetallic nanoparticles was also studied with scanning TEM (STEM) with 1 nm resolution, which provided the capability to identify the elemental distribution of the whole region of single nanoparticles before and after reactions at high temperature and a relatively high pressure. As shown in Figure 2b3,b4, the difference in the spatial distributions of Rh and Pd is clearly visible in the as-synthesized $Rh_{0.5}Pd_{0.5}$ nanoparticles. The comparison of top to bottom panels in Figure 10a shows a Pd-deficient surface region before any reactions. After reduction under 1 Torr H_2 at 300 °C, the atomic fraction of Pd increased in the surface region, on the basis of a comparison of the mapping configurations of Pd Kα and Rh Kα in the surface region of two single nanoparticles (marked with arrows in Figure 10b). The visible change in mapping configuration of the reacted nanoparticles is consistent with the increase of atomic fraction of Pd upon reduction of $Rh_{0.5}Pd_{0.5}$ nanoparticles, as measured with AP-XPS (Figure 6b).

3.3. Thermodynamic Equilibrium. Figure 11 shows the structural evolution of the $Rh_{0.5}Pd_{0.5}$ nanoparticles during a sequence of reactions following the introduction of nitric oxide at 300 °C. There was no further change of the surface composition of the restructured nanoparticles after 35 min (as shown in Figure 11) and at much longer times. This probably indicates that the phase formed in NO at 300 °C reached an equilibrium structure. When the nanoparticles were cooled to near room temperature in a gas environment of 0.1 Torr NO, no obvious change in the surface structure was observed (from reaction sequence 1 to 2 listed at the bottom of Figure 11). The

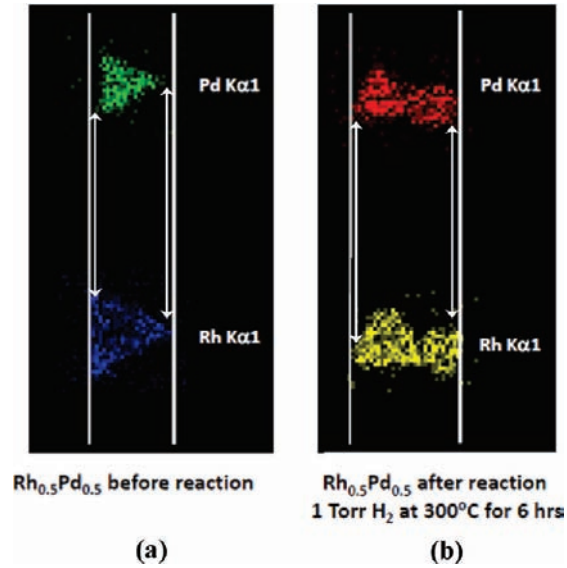

Figure 10. (a) Elemental mapping images of (top) Pd Kα and (bottom) Rh Kα for a representative as-synthesized $Rh_{0.5}Pd_{0.5}$ nanoparticle (~15 nm) before any reactions. The surface region of the nanoparticle is Pd-deficient. (b) Elemental mapping images of (top) Pd Kα and (bottom) Rh Kα for a representative as-synthesized $Rh_{0.5}Pd_{0.5}$ nanoparticle after reaction under 1 Torr H_2 at 300 °C for several hours. The atomic fraction of Pd in the surface region increased under reducing conditions. The white arrows in the two panels indicate the distribution of rhodium and palladium in the surface regions. The white arrows in (a) show the deficiency of Pd in the surface region of a representative $Rh_{0.5}Pd_{0.5}$ nanoparticle before reaction; the white arrows in (b) show the increased fraction of Pd in the surface region of a representative single $Rh_{0.5}Pd_{0.5}$ nanoparticle upon reduction under 1 Torr H_2 at 300 °C followed by cooling to room temperature under hydrogen.

Pd-rich surface structure remained unchanged after the catalyst was cooled from 317 °C to near room temperature under CO and the CO was purged to 1×10^{-7} Torr (from reaction sequence 4 to 5). No restructuring occurred for Pd-rich nanoparticles when the reaction environment was switched from reducing to oxidizing and the pressure was increased from 10^{-7} to 0.1 Torr at room temperature (from reaction sequence 5 to 6). Additional studies showed that no segregation of Rh or Pd occurred at temperatures below ~220 °C in environments of reducing or oxidizing reactants with a pressure of 0.1 Torr. This indicates that a different surface of bimetallic nanoparticles formed by restructuring at high temperatures (e.g., 300 °C) under certain pressures (e.g., 0.1 Torr) may be used for catalysis

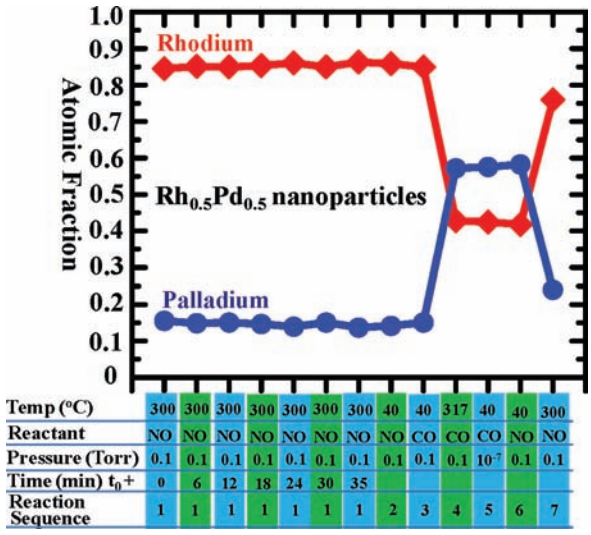

Temp (°C)	300	300	300	300	300	300	300	40	40	317	40	40	300
Reactant	NO	NO	NO	NO	NO	NO	NO	NO	CO	CO	CO	NO	NO
Pressure (Torr)	0.1	0.1	0.1	0.1	0.1	0.1	0.1	0.1	0.1	0.1	10^{-7}	0.1	0.1
Time (min) t_0+	0	6	12	18	24	30	35						
Reaction Sequence	1	1	1	1	1	1	1	2	3	4	5	6	7

Figure 11. Evolution of atomic fractions of rhodium and palladium in the restructured $Rh_{0.5}Pd_{0.5}$ nanoparticle catalyst (~15 nm) under a sequence of reaction conditions. The table below the figure lists the catalyst reaction temperatures, reactants, and pressures for a sequence of reactions.

performed at a temperature lower than the restructuring temperature. Notably, Pd nanoparticles possibly form the hydride under certain conditions.[26] However, there was no obvious amount of hydride formed in the Rh_xPd_{1-x} and Pd_xPt_{1-x} nanoparticles under conditions of 0.1 Torr H_2 at 300 °C based on the reported conditions.[26]

The observed reaction-driven changes in structure and chemistry of bimetallic nanoparticle catalysts demonstrate the importance of in situ studies of catalysts for understanding catalytic mechanisms at an atomic level. In addition, the understanding of the driving forces for surface restructuring of bimetallic nanoparticle catalysts during reactions is valuable for predicting the surface structure of bimetallic catalysts under reaction conditions. For example, Pd_xAu_{1-x}, which is a highly active catalyst for several reactions, such as hydrogen peroxide hydrogenation,[27] methane oxidation,[5] methanol fuel cell technologies,[27,28] and CO oxidation,[29,30] is expected to exhibit segregation of Pd and Au under oxidizing and reducing conditions, respectively. These possible changes in surface composition and oxidation states of the metal atoms under reaction conditions may help explain their composition-, structure-, and oxidation-state-dependent catalytic activities and selectivities.

4. Summary

Three series of bimetallic nanoparticle catalysts [Rh_xPd_{1-x} (~15 nm), Rh_xPt_{1-x} (8−11 nm), and Pd_xPt_{1-x} (~16 nm)] were synthesized via one-step reduction in solution under well-controlled reaction conditions. The combined average information from XPS of LB films of nanoparticle catalysts and local information from mapping configurations and EDX spectra of different *single* nanoparticles has allowed us to clearly identify the surface structure and atomic distribution of the bimetallic nanoparticle catalysts. Both the XPS depth profile and STEM mapping configuration showed that Rh_xPd_{1-x} and Pd_xPt_{1-x} nanoparticles exhibit an obvious significant dependence of the compositions of the two constituent elements on depth, whereas the as-synthesized Rh_xPt_{1-x} nanoparticles have a relatively homogeneous alloy Rh_xPt_{1-x} phase. Both Rh_xPd_{1-x} and Rh_xPt_{1-x} nanoparticles undergo reversible changes in surface composition and chemical states when the reaction conditions are changed from oxidizing to reducing or catalytic. However, no change in the distribution of Pd and Pt in the Pd_xPt_{1-x} nanoparticles was observed. The difference in restructuring behavior under the reaction conditions at 300 °C in these bimetallic nanoparticle catalysts may be rationalized by considering the surface free energy of the metals and the heat of formation of the metallic oxides. The observed structural changes in the nanoparticle catalysts under different reaction conditions demonstrate the importance of tracking the surface structure of nanomaterials such as nanocatalysts under working conditions. The restructuring exhibited by bimetallic nanoparticles suggests a method for developing catalysts by controllably restructuring the surface structure of as-synthesized nanoparticles.

Acknowledgment. This work was supported by the Director of the Office of Science, Office of Advanced Scientific Computing Research, Office of Basic Energy Sciences, Materials Sciences and Engineering Division, U.S. Department of Energy, under Contract DE-AC02-05CH11231.

JA101502T

(26) Yamauchi, M.; Ikeda, R.; Kitagawa, H.; Takata, M. *J. Phys. Chem. C* **2008**, *112*, 3294.
(27) (a) Maroun, F.; Ozanam, F.; Magnussen, O. M.; Behm, R. J. *Science* **2001**, *293*, 1811. (b) O'Hayre, R.; Colella, W.; Cha, S.-W.; Prinz, F. B. *Fuel Cell Fundamentals*; Wiley-VCH: Hoboken, NJ, 2009.
(28) Adzic, R. R.; Zhang, J.; Sasaki, K.; Vukmirovic, M. B.; Shao, M.; Wang, J. X.; Nilekar, A. U.; Mavrikakis, M.; Valerio, J. A.; Uribe, F. *Top. Catal.* **2007**, *46*, 249.
(29) Venezia, A. M.; Liotta, L. F.; Pantaleo, G.; La Parola, V.; Deganello, G.; Beckc, A.; Koppány, Z.; Frey, K.; Horváth, D.; Guczi, L. *Appl. Catal., A* **2003**, *251*, 359.
(30) Chen, M.; Kumar, D.; Yi, C. W.; Goodman, D. W. *Science* **2005**, *310*, 291.